Electronic Structure and Molecular Properties of the Heptacyanorhenate $[Re(CN)_7]^{3-}$ and $[Re(CN)_7]^{4-}$ Complexes

Jorge David,[†] Fernando Mendizábal,[‡] and Ramiro Arratia-Pérez*,[†]

Departamento de Ciencias Químicas, Universidad Andrés Bello, República 275, Santiago, Chile, and Departamento de Química, Facultad de Ciencias, Universidad de Chile, Casilla 653, Santiago, Chile

Received: October 14, 2005; In Final Form: November 23, 2005

We report scalar relativistic and Dirac scattered wave (DSW) calculations on the heptacyanorhenate $[Re(CN)_7]^{3-}$ and $Re(CN)_7^{4-}$ complexes. Both the ground and lowest excited states of each complex split by spin−orbit interaction by about 0.3 eV. The calculated molecular electronegativities χ indicate that the open-shell complex is less reactive than the closed-shell complex, in agreement with experimental observations. The calculations indicate that the ground state spin density is highly anisotropic and that spin−orbit effects are responsible for the magnetic anisotropy of the molecular **g** tensor of the $Re(CN)_7^{3-}$ complex. The calculated optical electronic transitions for both complexes with a polarizable continuum model using a time-dependent density functional (TDDFT)/B3LYP formalism are in reasonable agreement with those observed in the absorption spectrum.

I. Introduction

In recent years there has been great activity in the chemistry and properties of transition metal−cyanide complexes and clusters due to their possible use for an assortment of applications that include electronics, magnetism, and catalysis.[1,2] Thus, the title metal−cyanide complexes are viewed as useful molecular precursors, which can be incorporated into high-nuclearity clusters with adjustable magnetic properties and could be of utility in the design of cyano-bridged materials with potentially technological applications.[1−5] It is expected that the incorporation of third-row transition metal complexes may enhance the utility of such materials since these third-row transition metals possess higher-energy valence d orbitals that may induce magnetic anisotropy due to the effects of significant spin−orbit coupling.[4,5]

In particular, the low-spin (d^3) $[Re(CN)_7]^{3-}$ and (d^4) $[Re(CN)_7]^{4-}$ complexes have been structurally characterized.[3,6,7] The X-ray analysis of single crystals of $[Re(CN)_7]^{3-}$ and $[Re(CN)_7]^{4-}$ salts has indicated that both seven-coordinated complexes adopt a near pentagonal bipyramidal (D_{5h}) geometry.[3,6,7] The pentagonal bipyramidal (pbp) configuration for ML_7 complexes was predicted about three decades ago by Hoffmann et al. using an extended Hückel approach.[8]

In view of the current interest in metal−cyanide materials, we have investigated in this paper the electronic structure and spectral properties of both the above-mentioned rhenium−cyanide complexes using scalar relativistic and DSW calculations with the purpose of identifying relativistic and electron correlation effects on the ground and excited states of both complexes. We also performed time-dependent scalar density functional (TDDFT) calculations including solvent effects to rationalize their optical spectra and DSW first-order perturbational calculations to estimate the molecular **g** tensor of the (d^3) $[Re(CN)_7]^{3-}$ complex.

* Corresponding author. E-mail: rarratia@unab.cl.
[†] Universidad Andrés Bello.
[‡] Universidad de Chile.

II. Details of the Calculations

The geometry optimizations of each complex in a vacuum were carried out using the Amsterdam density functional code (ADF)[10] developed by Baerends and co-workers.[11−14] Electron correlation effects were treated within the LDA approximation, and nonlocal Becke exchange[15] and Perdew correlation gradient corrections[16] were included in the calculations. Solvation effects were estimated in a polarized continuum model (PCM)[17] of acetonitrile solutions using the Gaussian 98 package[18] with the B3LYP functional, where for Re the 15 valence electrons quasirelativistic pseudopotential of Andrae et al.[19] was employed, while for the C and N atoms, pseudopotentials using double-ζ basis sets with the addition of one d-type polarization function were employed.[20] The calculations of the excitation energies of each complex in a PCM were done at the B3LYP level using the time-dependent perturbation density functional theory approach (TDDFT).[21,22] Recent TDDFT calculations on metal hexacarbonyls using the B3LYP exchange−correlation functional and a continuum solvation model obtained quite accurate excitation energies.[23] The TDDFT approach provides an alternative to computationally demanding multireference configuration interaction methods for the calculation of excitation energies.

We also performed Dirac scattered wave (DSW) vectorial calculations to estimate spin−orbit effects and spin-dependent properties. In this formalism, an effective Coulomb and exchange−correlation potential approximate the Dirac four-component wave function as a Slater determinant.[24−29] The exchange−correlation potential is modeled by a relativistic local density potential according to MacDonald and Vosko.[30−32] For the calculation of the Zeeman magnetic splittings we start with a Dirac self-consistent four-component wave function Φ, and we employ a first-order perturbation procedure. The effects of an external magnetic field is described by a relativistic perturbation Hamiltonian $H_1 = e\,\alpha\cdot\mathbf{A}$, where α is the 4×4 Dirac matrix composed of zeros on the diagonal and the Pauli spin matrices in the off-diagonal positions, and **A** is the electromagnetic four-vector potential. When the magnetic nuclei is in the presence of an external magnetic field **B**, the four-vector potential is

10.1021/jp055884t CCC: $33.50
Published on Web 12/18/2005

TABLE 1: Group Relationships between the D_{5h} and D_{5h}* Point Groups

A. Group Compatibility Table

D_{5h}	A_1'	A_2'	E_1'	E_2'	A_1''	A_2''	E_1''	E_2''
D_{5h}*	Γ_9	Γ_9	$\Gamma_{10}+\Gamma_{12}$	$\Gamma_{11}+\Gamma_{13}$	Γ_{10}	Γ_{10}	$\Gamma_9+\Gamma_{11}$	$\Gamma_{12}+\Gamma_{13}$

B. Double Group Symmetry Allowed Electronic Transitions

$\Gamma_{11} \leftrightarrow \Gamma_{12}$ $\Gamma_{11} \leftrightarrow \Gamma_{13}$ $\Gamma_{11} \leftrightarrow \Gamma_{10}$ $\Gamma_{10} \leftrightarrow \Gamma_{13}$ $\Gamma_9 \leftrightarrow \Gamma_{10}$ $\Gamma_9 \leftrightarrow \Gamma_{12}$ $\Gamma_{13} \leftrightarrow \Gamma_{13}$

TABLE 2: Bond Lengths (Å) and Angles (deg) of the $[Re(CN)_7]^{3-}$ and $[Re(CN)_7]^{4-}$ Anions

	$[Re(CN)_7]^{3-}$			$[Re(CN)_7]^{4-}$		
	calc[a]	calc[b]	expt[c]	calc[a]	calc[b]	expt[d]
			(a) Distances			
$Re-C_{eq}$	2.11	2.14	2.09	2.12	2.15	2.09
$Re-C_{ax}$	2.09	2.14		2.10	2.15	2.08
$C-N_{eq}$	1.17	1.17	1.17	1.18	1.18	1.16
$C-N_{ax}$	1.18	1.17		1.18	1.18	1.16
			(b) Angles			
$C_{eq}-Re-C_{eq}$	72.0	72.0	72.4	72.0	72.0	71.9
$C_{ax}-Re-C_{eq}$	90.0	90.0	90.0	90.0	90.0	90.5
$Re-C-N$	180.0	180.0	178.6	180.0	180.0	173.4

[a] Gas phase optimization with ADF method. [b] Optimization in acetonitrile solutions with Gaussian98+B3LYP. [c] X-ray structure of $(Bu_4N)_3[Re(CN)_7]$, see ref 3. [d] X-ray structure of $K_4[Re(CN)_7]\cdot 2H_2O$, see ref 6.

represented by $\mathbf{A} = {}^1/_2(\mathbf{B} \times \mathbf{r})$, and, the Zeeman magnetic interactions are then described by the perturbation Hamiltonian $H_Z = {}^1/_2$ e $\alpha\cdot(\mathbf{B} \times \mathbf{r})$.[27-29,33] The $\langle\Phi|H_Z|\Phi\rangle$ matrix elements are evaluated in the basis spanning the "two" rows of the double-valued irreducible representations of the paramagnetic complex holding the single electron spin. Since the α matrices are off-diagonal, the evaluation of the matrix elements involves products of the "large" and "small" components of the Dirac wave function. The resulting perturbation energies are then fitted to the usual spin Hamiltonian $H_{spin} = \mathbf{S}\cdot\mathbf{g}\cdot\mathbf{B}$, where a convenient parametrized value of $\mathbf{S} = {}^1/_2$ is used to describe the ground state Kramers doublet, **g** being its associated **g** tensor.[28,33] Recent nonrelativistic molecular g tensor calculations at the CASSCF/CASPT2 level together with ligand field analysis were reported for the isolectronic (d^3) $Mo(CN)_7^{4-}$ complex under various geometries.[38]

To facilitate the analysis and understanding of our scalar relativistic calculations and Dirac scattered wave calculations, we provide in Table 1 the group relationships between the single (D_{5h}) and double (D_{5h}*) point groups.

III. Results and Discussion

The results of the geometry optimization performed in the vacuum and in a polarized continuum of acetonitrile solutions (PCM)[34,35] are listed in Table 2. It can be seen from Table 2 that the removal of one electron in $[Re(CN)_7]$,$^{4-}$ does not induce severe alterations in their geometries. The computed bond distances and bond angles, in both phases, are in reasonable agreement with the averaged experimental values.[3,6,7]

A. Molecular Orbitals. The ligands and metal interact through charge transfers among the 4σ, 5σ, 1π, and 2π* ligand cyanide orbitals and the rhenium s, p, and d orbitals. The metal−ligand bonding interactions are mainly governed by the usual mechanism of σ donation by the cyanide being accompanied by 2π* back-donation from the rhenium d orbitals.[36] Table 3 shows the total valence populations for both complexes given in terms of atomic spinors. It can be seen from this table that the rhenium 5d occupation is substantially larger than the value of 3 and 4 predicted by the d^3 and d^4 crystal field models. The same result is obtained from the scalar ADF calculations. This indicates net charge transfers of $\sim$0.4*e* and $\sim$0.3*e* per ligand molecule donated to the rhenium 5d orbitals, which form the metal−ligand bond. It is also possible to extract from Table 3 the ratios of occupied character for the $j = l - {}^1/_2$ and $j = l + {}^1/_2$ sublevels. In the nonrelativistic limit these ratios are required by symmetry to be $(l + 1)/l$, for $l > 0$. For d orbitals this nonrelativistic ratio is 1.50. The values of 1.21 and 1.33 obtained from Table 3 for the rhenium valence 5d orbitals indicate that the $d_{3/2}$ orbitals are clearly favored over $d_{5/2}$, as expected for a relatively large spin−orbit coupling constant.

TABLE 3: Total Valence Populations (electrons/atom)

atom	l	j	$[Re(CN)_7]^{3-}$	$[Re(CN)_7]^{4-}$
Re	0	1/2	0.604	0.591
Re	1	1/2	0.317	0.311
Re	1	3/2	0.529	0.524
Re	2	3/2	2.686	2.677
Re	2	5/2	3.256	3.574
total			7.392	7.677
C_{ax}	0	1/2	1.214	1.228
C_{ax}	1	1/2	0.956	0.952
C_{ax}	1	3/2	1.892	1.890
total			4.062	4.070
N_{ax}	0	1/2	1.372	1.367
N_{ax}	1	1/2	1.336	1.344
N_{ax}	1	3/2	2.602	2.692
total			5.310	5.403
C_{eq}	0	1/2	1.209	1.227
C_{eq}	1	1/2	0.950	0.949
C_{eq}	1	3/2	1.889	1.884
total			4.048	4.060
N_{eq}	0	1/2	1.384	1.381
N_{eq}	1	1/2	1.313	1.343
N_{eq}	1	3/2	2.629	2.691
total			5.326	5.415

The calculated energy gaps between the occupied and unoccupied states of both complexes are large ($\sim$4.0 eV), so that it is a good approximation to represent their ground states as a single determinant. Under a pentagonal bipyramidal (pbp) crystal field, the rhenium d orbitals split (and are populated) in $[Re(CN)_7]^{3-}$ according to $(de_1'')^{2.97}$ $(de_2')^{1.87}$ $(da_1')^{0.76}$ as calculated by the ADF code, while, the calculation by the DSW code gives $(de_1'')^{3.16}$ $(de_2')^{1.84}$ $(da_1')^{0.92}$, respectively. Similarly, the d-splitting and populations in $[Re(CN)_7]^{4-}$ are $(de_1'')^{3.23}$ $(de_2')^{1.67}$ $(da_1')^{0.87}$, as calculated by the ADF code, while the calculation by the DSW code gives $(de_1'')^{3.45}$ $(de_2')^{1.85}$ $(da_1')^{0.95}$, respectively. It can be inferred from Table 1 that de_1'' transforms as $d(\gamma_9 + \gamma_{11})$, de_2' as $d(\gamma_{11} + \gamma_{13})$, and da_1' as $d\gamma_9$.

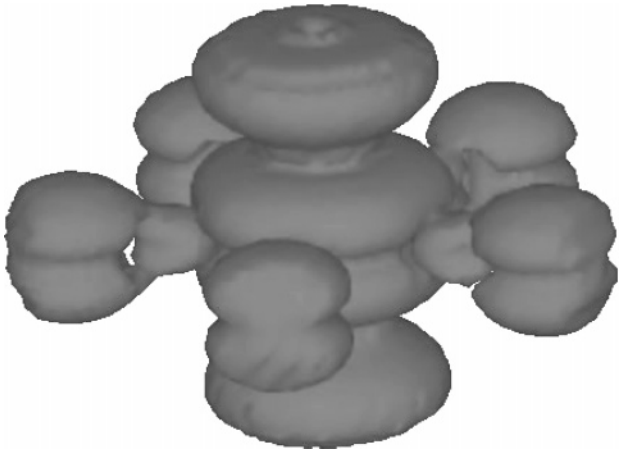

Figure 1. Relativistic three-dimensional (3D) spin density plot (electron/bohr^3)$^{3/2}$ of the $Re(CN)_7^{3-}$ complex.

TABLE 4: TD-DFT/B3LYP Singlet-Excitation Calculations for $[Re(CN)_7]^{3-}$ in MeCN Solution Phase (PCM)

λ_{calc} (nm)	f[a]	λ_{exp} (nm)	ϵ[b]	contributions[c]	type transition
394.6	0.0094	395	1280	$36E_1' \beta \rightarrow 41A_2'' \beta$ (98.5)	LMCT ($\pi^* \rightarrow$ dyz)
364.0	0.0440	363	899	$33E_1'' \beta \rightarrow 41A_2'' \beta$ (97.4)	LMCT ($\pi \rightarrow$ dyz)
350.7	0.0146	326	1620	$32E_2'' \beta \rightarrow 41A_2'' \beta$ (96.4)	LMCT ($\pi \rightarrow$ dyz)
350.7	0.0157	315	2030	$31E_2'' \beta \rightarrow 41A_2'' \beta$ (96.3)	LMCT ($\pi^* \rightarrow$ dyz)
291.4	0.0217	293	2620	$26A_2'' \beta \rightarrow 41A_2'' \beta$ (96.9)	LMCT ($\pi \rightarrow$ dyz)
241.6	0.0137	258	2280	$40E_1'' \beta \rightarrow 45E_1' \beta$ (62.1)	MMCT (dxz $\rightarrow p_z$)
				$40E_1'' \beta \rightarrow 48E_1'' \beta$ (20.7)	MLCT (dxz $\rightarrow \pi^*$)
233.2	0.0119	233	8390	$40E_1'' \beta \rightarrow 47A_2'' \beta$ (99.5)	MMCT (dxz $\rightarrow p_x$)

[a] Oscillator strength. [b] Molar extinction coefficient in L mol^{-1} cm^{-1} in MeCN. [c] Value is $|coeff.|^2 \times 100$.

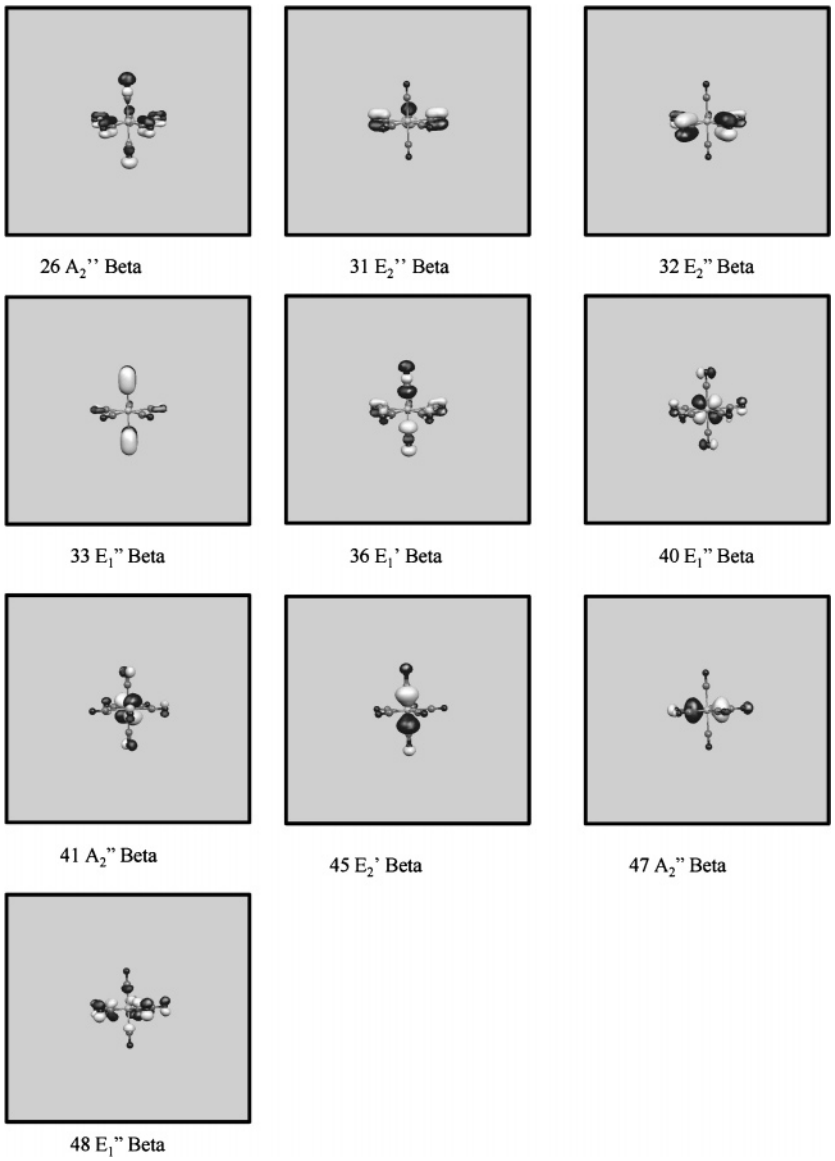

Figure 2. Active molecular orbitals of the $Re(CN)_7^{3-}$ complex. The SOMO is $40E_1''$.

The HOMO of each component of the $[Re(CN)_7]^{3-/4-}$ redox couple spans the e_1'' symmetry representation and, in both cases, arises primarily (~70%) from the metal ($5de_1''$) and the rest arises from the axial and equatorial nitrogens. Spin−orbit coupling splits these HOMOs e_1'' levels into ($\gamma_9 + \gamma_{11}$) by 0.28 eV (~2250 cm^{-1}) in both complexes. A similar spin−orbit splitting ($5dt_{2g}$) of 0.26 eV has been observed and calculated in $W(CO)_6$.[36,37] Thus, according to our calculations the $[Re(CN)_7]^{3-}$ ion is paramagnetic characterized by a Kramer doublet of γ_{11} symmetry, while the $[Re(CN)_7]^{4-}$ ion is diamagnetic characterized by a singlet ground state. The LUMO in both complexes, however, spans the e_2' symmetry representation which arises primarily from contributions of the equatorial ligands but mixed with about 30% 5d rhenium content. In both complexes, the unoccupied degenerated e_2' levels split by spin−orbit interaction into ($\gamma_{11} + \gamma_{13}$) by about 0.30 eV (~2400 cm^{-1}). The PCM-B3LYP calculation places an energy level of a_2'' symmetry very close to the LUMO e_2'. Therefore, the ground and first-excited states of both rhenium complexes split by spin−orbit interaction involving the $5d_{3/2,5/2}$ spinors.

The calculated molecular electronegativities[26] (χ) of the paramagnetic $[Re(CN)_7]^{3-}$ ($\chi = 8.0$ eV) and of the diamagnetic

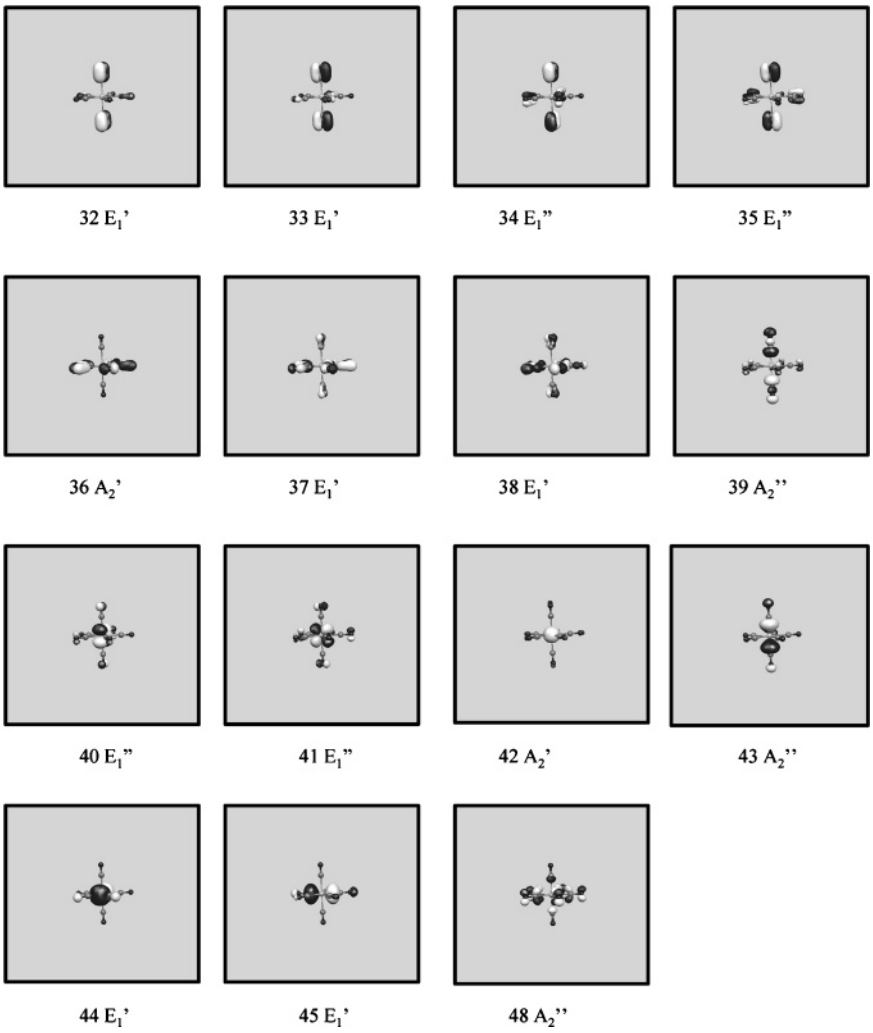

Figure 3. Active molecular orbitals of the $Re(CN)_7^{4-}$ complex. The HOMO is $41E_1''$.

TABLE 5: TD-DFT/B3LYP Singlet-Excitation Calculations for $[Re(CN)_7]^{4-}$ in MeCN Solution Phase (PCM)

λ_{calc} (nm)	f[a]	contributions[b]	type transition
320.3	0.0272	$41E_1'' \rightarrow 43A_2''$ (99.6)	MMCT (dxz → p_z)
320.3	0.0272	$40E_1'' \rightarrow 43A_2''$ (99.6)	MMCT (dyz → p_z)
314.3	0.0363	$40E_1'' \rightarrow 44E_1''$ (69.4)	MMCT (dyz → p_y)
		$41E_1'' \rightarrow 45E_1'$ (30.1)	MMCT (dxz → p_x)
314.3	0.0363	$40E_1'' \rightarrow 44E_1''$ (30.1)	MMCT (dyz → p_y)
		$41E_1'' \rightarrow 45E_1'$ (69.4)	MMCT (dxz → p_x)
247.8	0.0779	$41E_1'' \rightarrow 48A_2''$ (93.6)	MLCT (dxz → π^*)
247.8	0.0779	$40E_1'' \rightarrow 48A_2''$ (93.6)	MLCT (dyz → π^*)
211.5	0.0224	$39E_2'' \rightarrow 42A_1'$ (95.5)	LMCT ($\pi^* \rightarrow$ 6s)
211.0	0.0087	$38E_1' \rightarrow 42A_1'$ (95.5)	LMCT ($\pi^* \rightarrow$ 6s)
211.0	0.0087	$37E_1' \rightarrow 42A_1'$ (95.5)	LMCT ($\pi^* \rightarrow$ 6s)
195.7	0.0037	$33E_1' \rightarrow 42A_1'$ (88.1)	LMCT ($\pi^* \rightarrow$ 6s)
		$35E_1'' \rightarrow 43A_2''$ (6.1)	LMCT ($\pi^* \rightarrow p_z$)
		$36A_2' \rightarrow 44E_1'$ (3.7)	LMCT ($\pi^* \rightarrow p_y$)
195.7	0.0037	$32E_1' \rightarrow 42A_1'$ (88.1)	LMCT ($\pi^* \rightarrow$ 6s)
		$34E_1'' \rightarrow 43A_2''$ (6.1)	LMCT ($\pi^* \rightarrow p_z$)
		$36A_2' \rightarrow 45E_1'$ (3.7)	LMCT ($\pi^* \rightarrow p_x$)

[a] Oscillator strength. [b] Value is $|\text{coeff.}|^2 \times 100$.

$[Re(CN)_7]^{4-}$ ($\chi = 3.3$ eV) complexes clearly suggest that $[Re(CN)_7]^{4-}$ is more reactive than $[Re(CN)_7]^{3-}$. Considering that χ measures the escaping tendency of the electron cloud, the calculated χ indicates that the closed-shell complex is more reactive than the open-shell complex. This is consistent with the fact that the paramagnetic $[Re(CN)_7]^{3-}$ complex is stable in air both in solid state and in nonprotic solvents. In contrast, the diamagnetic $[Re(CN)_7]^{4-}$ complex rapidly oxidizes in air.[3] Moreover, the cyclic voltammogram of $(Bu_4N)_3[Re(CN)_7]$ in acetonitrile displays a quasireversible $[Re(CN)_7]^{3-/4-}$ redox couple centered at $E_{1/2} = -1.06$ V vs $Cp_2Fe^{0/1}$.[3,40]

B. Electron Spin Distribution and Molecular g Tensor of $Re(CN)_7^{3-}$. In relativistic theory, the spinors with $j = {}^1/_2$ give rise to isotropic spin distributions (ρ_{iso}), and the spinors with $j > {}^1/_2$ give rise to anisotropic spin distributions (ρ_{aniso}). In the case of the paramagnetic $Re(CN)_7^{3-}$ complex, a unit electron spin distribution should obey the following: $\rho(Re) + 2\rho(C_{ax}) + 2\rho(N_{ax}) + 5\rho(C_{eq}) + 5\rho(C_{eq}) = 1.000$.[33,39] Proceeding in this manner, we obtained the following electron spin distribution: $\rho_{aniso}(Re) = 0.690$, $\rho_{aniso}(C_{ax}) = 0.014$, $\rho_{aniso}(N_{ax}) = 0.146$, $\rho_{aniso}(C_{eq}) = 0.010$, $\rho_{iso}(N_{eq}) = 0.050$, and $\rho_{aniso}(N_{eq}) = 0.090$. Thus, our relativistic calculations indicate that the electron spin density of the paramagnetic $Re(CN)_7^{3-}$ complex is mostly anisotropic, in which the unpaired electron spin spends about 69% of its time associated with the rhenium 5d orbitals. This can be visualized from Figure 1, where we show the relativistic three-dimensional (3D) spin density plot of the $Re(CN)_7^{3-}$ complex. Currently, efforts are underway to obtain the spin density of this paramagnetic complex by neutron diffraction techniques.[40]

The DSW and scalar relativistic (ZORA)[13-15] calculations of the **g** tensor of the $Re(CN)_7^{3-}$ complex predict an axial and anisotropic **g** tensor with values of $\mathbf{g}_{\parallel} = 3.24$ and 3.54 and $\mathbf{g}_{\perp} = 0.00$ and 0.00, respectively. However, the X-band EPR spectrum of an undiluted powder of $(Bu_4N)_3[Re(CN)_7]$ at 20 K is axial

and anisotropic with $\mathbf{g}_{\parallel} = 3.66$ and $\mathbf{g}_{\perp}=1.59$.[3] The difference between calculated and measured $\mathbf{g}_{\perp}$ tensor component could be ascribed to deviations of the actual geometry of the complex from the ideal pentagonal bipyramidal (D_{5h}) geometry. By examining the crystallographic information file (CIF) of the $(Bu_4N)_3[Re(CN)_7]$ compound,[40] it is possible to see that three of the equatorial CN units and the Re atom have a planar conformation with a small deviation from the "best plane". The other two equatorial CN units are above and below the "best plane" showing a significant deviation. Furthermore, the plane containing these two CN units and the Re atom form an angle of 10.47° with the "best plane". On the other hand, the angle between one axial CN unit, the Re atom, and the other axial CN is approximately 178°. Obviously, significant distortions will induce magnetic moments in the equatorial plane resulting in nonzero values of $\mathbf{g}_{\perp}$. It should be pointed out that the ESR spectrum was taken on an undiluted powder sample; however, it will be highly desirable to perform a single-crystal EPR experiment for $Re(CN)_7^{3-}$. A similar difference between calculated and measured $\mathbf{g}_{\perp}$ tensor component was recently detected for the isoelectronic and isostructural $Mo(CN)_7^{4-}$ complex.[38] The large deviation of the molecular **g** tensor components from the spin-only value arises from the effects of spin−orbit coupling that splits the $^2E_1''$ ground state of $Re(CN)_7^{3-}$ by 0.28 eV.

C. Optical Properties. The excitation energies were obtained at the B3LYP level from single-point calculations of the pbp models in a PCM using the time-dependent perturbation theory approach (TD-DFT).[21,22,23] The allowed spin singlet transition for these complexes was calculated based on the ground state structures of the pbp models. The objective was to evaluate the electronic structure of the excited states by direct electronic excitations. Only singlet−singlet transitions were considered in these scalar relativistic calculations. The allowed transitions are shown in Tables 4 and 5. Here, we considered as permitted or allowed transitions those whose oscillator strength is nonzero. The molecular orbitals active in the electronic transitions are depicted in Figures 2 and 3.

$[Re(CN)_7]^{3-}$. The calculated optical transitions in acetonitrile and the experimental absorption spectroscopic data in acetonitrile are summarized in Table 4. The experimental spectrum shows an intense absorption band (with a large molar extinction coefficient) at 233 nm ($\epsilon_M = 8390$), which is estimated theoretically at 233.2 nm. This band could be assigned as the $40E_1' \rightarrow 47A_2''$ transition, mainly associated with MMCT $d_{xz} \rightarrow p_x$ character. This transition is also double-group symmetry allowed (see Table 1). The remaining calculated transitions are in reasonable agreement with the experimental bands, mainly associated with bands of LMCT character (see Table 4 and Figure 2). In general, there is reasonable agreement with the experimental data.

$[Re(CN)_7]^{4-}$. There are not reported measurements of the electronic spectrum of this system. Thus, our results reported here have predictive character. The calculated optical transitions in acetonitrile are summarized in Table 5. Most of the transitions are doubly degenerated. In qualitative terms, we can distinguish three regions: (i) transitions between 320.3 and 314.2 nm, corresponding to MMCT type; (ii) a stronger transition at 247.8 nm associated with MLCT of the type $41E_1''$ (d_{xz}) → $48A_2''$ (π^*) and $40E_1''$ (d_{yz}) → $48A_2''$ (π^*) (see OMs in Figure 3); and (iii) lower transitions between 211.5 and 195.7 nm assigned as LMCT type.

IV. Conclusions

The present study has demonstrated that scalar relativistic and DSW calculations could explain adequately the optical and magnetic properties of third-row transition metal cyanide complexes. We found that both the ground and lowest excited states of each heptacyanorhenate complex split by spin−orbit interaction by about 0.3 eV. The calculated molecular electronegativities χ suggest that the open-shell complex is less reactive than the closed-shell complex, in agreement with experimental observations. Spin−orbit effects are responsible for the magnetic anisotropy of the molecular **g** tensor of the paramagnetic $Re(CN)_7^{3-}$ complex. The large deviation of the molecular **g** tensor components from the spin-only value arises from the effects of spin−orbit coupling that split the $^2E_1''$ ground state of $Re(CN)_7^{3-}$. The calculations also indicated that the ground state spin density is highly anisotropic. Thus, due to its large magnetic anisotropy, the $Re(CN)_7^{3-}$ complex can be a useful molecular precursor for the design of new magnetic materials. The calculated optical electronic transitions for both complexes in a polarizable continuum model using a time-dependent density functional (TDDFT)/B3LYP formalism are in reasonable agreement with those observed in the absorption spectrum.

Acknowledgment. R.A.P. sincerely thanks Jeffrey Long for valuable discussions. We thank Luis Alvarez-Thon for analyzing the CIF file. This work has been supported in part by Fondecyt No.1030148, Fondecyt 1020141, UNAB-DI 12-04, UNAB-DI 20-04, and the Millennium Nucleus of Applied Quantum Mechanics and Computational Chemistry, P02-004-F.

References and Notes

(1) (a) Ferlay, S.; Mallah, T.; Ouahes, R.; Veillet, P.; Verdaguer, M. *Nature* **1995**, *378*, 701. (b) Dunbar, K. R.; Heintz, R. A. *Prog. Inorg. Chem.* **1997**, *45*, 283. (c) Yet, L. *Angew. Chem., Int. Ed. Engl.* **2001**, *40*, 875.

(2) (a) Khan, O.; Martinez, C. J. *Science* **1998**, *279*, 44. (b) Berlinguette, C. P.; Smith, J. A.; Galan-Mascaros, J. R.; Dunbar, K. R. *C. R. Chimie* **2002**, *5*, 665.

(3) Bennett, M. V.; Long, J. R. *J. Am. Chem. Soc.* **2003**, *125*, 2394.

(4) Sokol, J. J.; Hee, A. G.; Long, J. R. *J. Am. Chem. Soc.* **2002**, *124*, 7656.

(5) Beltran, L. M. C.; Long, J. R. *Acc. Chem. Res.* **2005**, *38*, 325.

(6) Manoli, J. M.; Potvin, C.; Bregeault, J. M. *J. Chem. Soc., Dalton Trans.* **1980**, 192.

(7) Griffith, W. P.; Kiernan, P. M.; Bregeault, J. M. *J. Chem. Soc., Dalton Trans.* **1978**, 1411.

(8) Hoffmann, R.; Beier, B. F.; Muetterties, E. L.; Rossi, A. R. *Inorg. Chem.* **1977**, *16*, 511.

(9) Hendrickx, M. F. A.; Mironov, V. S.; Chitobaru, L. F.; Ceulemans, A. *Inorg. Chem.* **2004**, *43*, 3142.

(10) *Amsterdam Density Functional (ADF) code*, release 2004; Vrije Universiteit: Amsterdam, The Netherlands, 2004.

(11) Baerends, E. J.; Ellis, D. E.; Ros, P. *Chem. Phys.* **1973**, *2*, 41.

(12) te Velde, G.; Baerends, E. J. *J. Comput. Phys.* **1992**, *99*, 84.

(13) Boerrigter, P. M.; te Velde, G.; Baerends, E. J. *Int. J. Quantum Chem.* **1998**, *33*, 87.

(14) te Velde, G.; Bickelhaupt, F. M.; Van Gisbergen, S. J. A.; Fonseca Guerra, C.; Baerends, E. J.; Snijders, J. G.; Ziegler, T. *J. Comput. Chem.* **2001**, *22*, 931.

(15) Becke, A. D. *Phys. Rev. A* **1988**, *38*, 3098.

(16) Perdew, J. P. *Phys. Rev. B* **1986**, *33*, 8822. Perdew, J. P. *Phys. Rev. B* **1986**, *34*, 7046.

(17) Cossi, M.; Barone, V. *J. Phys. Chem. A* **1998**, *102*, 1995.

(18) Frisch, M. J. et al., *Gaussian 98 rev. A.11*; Pittsburgh, PA, 2002.

(19) Andrae, D.; Hausserman, U.; Dolg, M.; Stoll, H.; Preuss, H. *Theor. Chim. Acta* **1990**, *77*, 123.

(20) Bergner, A.; Dolg, M.; Kuchle, W.; Stoll, H.; Preuss, H. *Mol. Phys.* **1993**, *80*, 1431.

(21) Bauernschmitt, R.; Ahlrichs, R. *Chem. Phys. Lett.* **1996**, *256*, 454.

(22) Casida, M. E.; Jamorski, C.; Casida, K. C.; Salahub, D. R. *J. Chem. Phys.* **1998**, *108*, 4439.

(23) Hummel, P.; Oxgaard, J.; Goddard, W. A., III; Gray, H. B. *Inorg. Chem.* **2005**, *44*, 2454.

(24) Yang, C. Y.; Case, D. A. In *Local density approximations in quantum chemistry and solid-state physics*; Dahl, J. P., Avery, J., Eds.; Plenum: New York, 1983.
(25) Arratia-Pérez, R.; Hernández-Acevedo, L. *J. Chem. Phys*. **1999**, *110*, 2529.
(26) (a) Vera, L.; Zuloaga, F. *J. Phys. Chem*. **1984**, *88*, 6415. (b) Arratia-Pérez, R.; Hernández-Acevedo, L. *J. Chem. Phys*. **1999**, *111*, 168.
(27) Alvarez-Thon, L.; Hernández-Acevedo, L.; Arratia-Perez, R. *J. Chem. Phys*. **2001**, *115*, 726.
(28) Arratia-Pérez, R.; Hernández-Acevedo, L. *J. Chem. Phys*. **2003**, *118*, 7425.
(29) Arratia-Pérez, R.; Hernández-Acevedo, L.; Malli, G. L. *J. Chem. Phys*. **2004**, *121*, 7743.
(30) MacDonald, A. H.; Vosko, S. H. *J. Phys. C* **1979**, *12*, 2977.
(31) Rajagopal, A. K. *J. Phys. C* **1978**, *11*, L943.
(32) Rajagopal, A. K. *Adv. Chem. Phys.* **1980**, *41*, 59.
(33) Harriman, J.E. *Theoretical Foundations of Electron Spin Resonance*; Academic Press: New York, 1978.
(34) Miertus, S.; Scrocco, E.; Tomasi, J. *Chem. Phys*. **1981**, *55*, 117.
(35) Cossi, M.; Barone, V.; Cammi, R.; Tomasi, J. *Chem. Phys. Lett*. **1996**, *255*, 327.
(36) Hubbard, J. L.; Lichtenberger, D. L. *J. Am. Chem. Soc*. **1982**, *104*, 2132.
(37) Arratia-Perez, R.; Yang, C. Y. *J. Chem. Phys.* **1985**, *83*, 4005.
(38) Chibotaru, L. F.; Hendrickx, M. F. A.; Clima, S.; Larionova, J.; Ceulemans, A. *J. Phys. Chem. A* **2005**, *109*, 7251.
(39) Weltner, W., Jr. *Magnetic Atoms and Molecules*; Dover: New York, 1989.
(40) Long, J. R. Private communication.